Geomechanics and Engineering, *Vol. 30, No. 2 (2022) 169-185*
DOI: https://doi.org/10.12989/gae.2022.30.2.169

A parametric study of settlement and load transfer mechanism of piled raft due to adjacent excavation using 3D finite element analysis

Hemu Karira*[1], Aneel Kumar[2], Tauha Hussain Ali[2], Dildar Ali Mangnejo[1] and Naeem Mangi[3]

[1]*Department of Civil Engineering, Mehran University of Engineering and Technology, Shaheed Zulfiqar Ali Bhutto Campus, Khairpur Mir's, Sindh, Pakistan*
[2]*Department of Civil Engineering, Mehran University of Engineering and Technology, Jamshoro, Sindh, Pakistan*
[3]*Department of Civil Engineering, Quaid-e-Awam University of Engineering, Science & Technology, Sindh, Pakistan*

(Received April 24, 2022, Revised June 2, 2022, Accepted June 26, 2022)

Abstract. The urbanization and increasing rate of population demands effective means of transportation system (basement and tunnels) as well as high-rise building (resting on piled foundation) for accommodation. Therefore, it unavoidable to construct basements (i.e., excavation) nearby piled foundation. Since the basement excavation inevitably induces soil movement and stress changes in the ground, it may cause differential settlements to nearby piled raft foundation. To understand settlement and load transfer mechanism in the piled raft due to excavation-induced stress release, numerical parametric studies are carried out in this study. The effects of excavation depths (i.e., formation level) relative to piled raft were investigated by simulating the excavation near the pile shaft (i.e., H_e/L_p=0.67), next to (H_e/L_p=1.00) and below the pile toe (H_e/L_p=1.33). In addition, effects of sand density and raft fixity condition were investigated. The computed results have revealed that the induced settlement, tilting, pile lateral movement and load transfer mechanism in the piled raft depends upon the embedded depth of the diaphragm wall. Additional settlement of the piled raft due to excavation can be account for apparent loss of load carrying capacity of the piled raft (ALPC). The highest apparent loss of piled raft capacity ALPC (on the account of induced piled raft settlement) of 50% was calculated in in case of H_e/L_p = 1.33. Furthermore, the induced settlement decreased with increasing the relative density from 30% to 90%. On the contrary, the tilting of the raft increases in denser ground. The larger bending moment and lateral force was induced at the piled heads in fixed and pinned raft condition.

Keywords: excavation; fixity condition; parametric study; piled raft; sand density

1. Introduction

In densely built urban cities, the rapidly increasing population demands an effective means of underground transportation system (Hong *et al.* 2017, Shi *et al.* 2015, Soomro *et al.* (2022a, b). The underground transportation system consists of tunnels, basements and subway metro stations. These excavations are sometimes inevitable to be constructed adjacent to existing piled foundations. In urban areas many high buildings are supported by piled rafts because the use of piles to reduce raft settlements and differential settlements can lead to considerable economy without compromising the safety and performance of the foundation (Bai *et al.* 2021). Since the underground basement excavation inevitably induces soil movement and stress changes in the ground, it may cause additional settlement and differential settlements to nearby existing piled foundations. This condition leads to a big challenge for a geotechnical engineer to assess and protect the integrity of piled foundation. Many studies have investigated the effects of stress release and horizontal soil movements on existing piles (Finno *et al.* 1991, Liyanapathirana and Nishanthan 2016, Goh *et al.* 2003). In soft clay, Ong *et al.* (2006, 2009) conducted centrifuge tests to evaluate the excavation induced lateral responses of end bearing single piles (SP) and pile groups (PG), respectively. They reported that the distance of the piles from the excavation and showing effects of the piles in a group influenced the lateral deflection and bending moments of the piles. Both studies were focused on the end bearing piles, and the settlement response of floating pile foundations was not investigated. However, the settlement response of floating piles is critical for the serviceability of pile-supported structures. The structures supported by floating pile foundations would experience severe damages due to excessive pile settlement and tilting (Korff *et al.* 2016) caused by the stress release and vertical soil movements, which has not yet been fully characterized. Some previous studies have investigated the excavation induced settlement of the floating pile. (Korff *et al.* 2016, Ng *et al.* 2017, Shi *et al.* 2019, Soomro *et al.* 2021a, Tan *et al.* 2016, Zhang *et al.* 2011). Korff *et al.* (2016) presented design charts to estimate the settlement of SP considering greenfield soil settlement using the analytical solution and two-stage continuum-based non-linear model, respectively.

These studies proposed a framework to determine the interaction level (z_i where greenfield soil settlement becomes equal to the pile settlement) considering the influence of the initial factor of safety (FS). The interaction level moves upward with the decrease of FS, resulting in

*Corresponding author, Ph.D. Student
E-mail: HemuKarira@muetkhp.edu.pk

http://www.techno-press.org/?journal=gae&subpage=7
ISSN: 2005-307X (Print), 2092-6219 (Online)

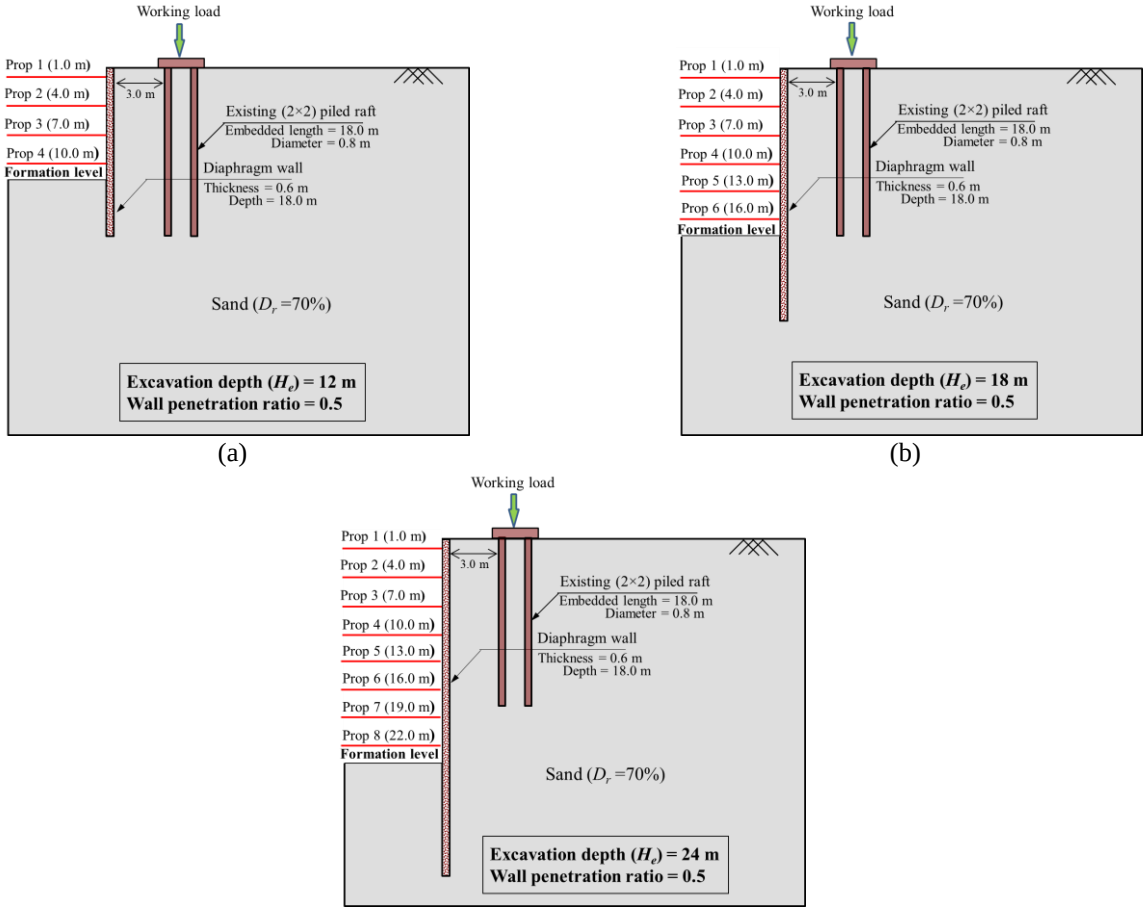

Fig. 1 Configuration of numerical simulations of three cases (a) H_e/L_p =0.67, (b) H_e/L_p =1.00 and (c) H_e/L_p = 1.33

larger excavation-induced pile settlement. These studies consider the greenfield soil movements in the uniform ground and neglect the influence of effective stress changes due to excavation-induced stress release or excess pore water pressure. Furthermore, these studies were limited to single pile interaction scenarios and ignored the effects of group interaction and load redistribution between the piles on excavation-induced pile settlement. Shi *et al.* (2019) and Soomro *et al.* (2021d) presented excavation-induced settlement of nearby floating SP in sand and clay, respectively, using finite element analysis. They found that excavation had a significant influence on SP settlement. These studies are limited to SP response, and the findings are not applicable for PG due to group interaction and load redistribution between the piles. Ng *et al.* (2021) investigated the settlement and tilting mechanism due to deep excavation of a (2×2) pile group in dry sand using the centrifuge and numerical modelling. They found that PG settlement and tilting are proportional to the excavation depth, and the front pile experiences a larger settlement than the rear pile. Ng *et al.* (2021) conducted a series of three-dimensional (3D) centrifuge model tests and numerical simulations to investigate the influence of raft contact on the response of an existing (2×2) piled raft in comparison to that of an elevated pile group when subjected to an adjacent multipropped deep excavation in dry sand. They concluded that 20% larger settlement was seen in the piled raft foundation than in the pile group, to further mobilize shaft and end bearing resistances for the maintenance of vertical equilibrium. Apart from Ng *et al.* 2021's study, authors are not aware of any other research related to effects of excavation of piled raft in the literature. Therefore, there is a lack of systematic research on the behaviour of an existing pile raft due to excavation. This paper aims to understand the responses of (2×2) piled raft to ground movement due to excavation-induced stress relief. To achieve this, three-dimensional finite element analysis was conducted. Moreover, three-dimensional numerical parametric studies were conducted to systematically investigate settlement and load transfer mechanism induced in the piled raft due to a multi-propped excavation. Various combinations of excavation depth systems, sand density and raft fixity conditions were taken into consideration the numerical parametric study.

2. Three-dimensional finite element analysis

2.1 Numerical modelling programme

Three-dimensional finite element approach was used to investigate settlement and load transfer mechanism of piled raft due to excavation. To explore the effects of different excavation depth systems, three different final excavation

Table 1 Summary of numerical simulations in the parametric study

Variable	Excavation depth (m)	Diaphragm wall depth (m)	Raft fixity condition	Relative density of sand: %	Objective
Load test	N/A	N/A	N/A	70	Piled raft load test
Excavation & wall depth	12.0 18.0 24.0	18.0 24.0 36.0	Free	70	Effects of excavation depths
Sand density	12, 18 & 24	18, 24 & 36	Free	30 50 70 90	Effects of relative density of sand
Raft fixity condition	24	36	Free Pinned fixed	70	Effects raft fixity conditions

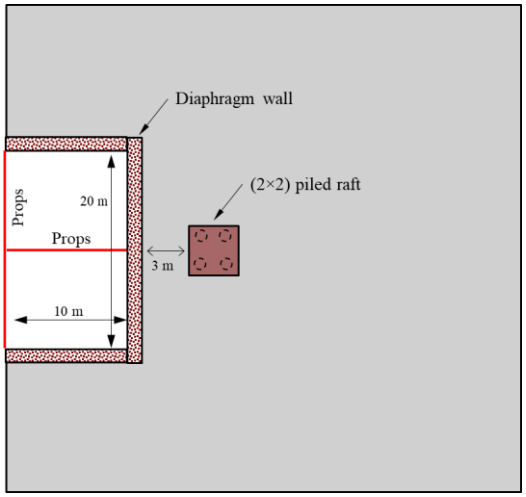

Fig. 2 Plan view of a typical case of H_e/L_p =0.67

depths (H_e) relative to the pile length (L_p) namely near the pile shaft (H_e/L_p = 0.67), adjacent to the pile toe (H_e/L_p = 1.00) and below the pile toe (H_e/L_p = 1.33) were taken in this parametric study. The final depth of the excavation (H_e) has been adopted as 12 m, 18 m and 24 m in case of H_e/L_p = 0.67, 1.00 and 1.33, respectively. The embedded length (L_p) and diameter (d_p) of the pile are 18 m and 0.8 m, respectively. The modelled pile represents a cylindrical reinforced concrete (grade 40, reinforcement ratio = 1) with a bending moment capacity of 800 kNm. Figs. 1(a)-1(c) show the elevations views of the configurations of numerical simulations of H_e/L_p = 0.67, H_e/L_p = 1.00 and H_e/L_p = 1.33, respectively. To simulate long and narrow metro stations, a basement with a final excavation depth (H_e) of 25.0 m and a width of 10.0 m was simulated in the numerical analysis, while excavation length was taken as 20 m as illustrated in Fig. 2. The clear distance between diaphragm wall and the pile is 3.0 m. The excavation was supported by 0.6 m thick diaphragm wall. The ratio of wall penetration depth to excavation depth is typically 0.5-2 in engineering practice (Hsiung 2009, Ng *et al.* 2017, Shi *et al.* 2019, Xue *et al.* 2021, Wang *et al.* 2022), thus a value of 0.5 is adopted in this study. The props are used to support the diaphragm wall with a vertical spacing of 3 m. The props (I-section) are modelled as soft with axial rigidity of 81 × 10^3 kNm (Hsiung 2009). Horizontal spacing of props is 10 m. It is evident from the research available in literature that the stiffness of the sand is mainly depend upon relative density (Shi *et al.* 2019) and pile head fixity condition (i.e., free, pinned and fixed) has significant effect on the pile response to excavation (Liyanapathirana and Nishanthan 2016, Ng *et al.* 2017, Hu *et al.* 2021, 2022) Hence, the analyses investigating the excavation effects on the piled raft constructed in sand with three different relative density (i.e., D_r = 30%, 50%, 70% and 90%) and different piled raft head conditions were added in this parametric study. To investigate the pile head fixity conditions at different excavation depths, the three boundary conditions (*i*) free in which both translation and rotation are allowed, (*ii*) pinned in which translation is constraint and rotation is allowed and (*iii*) fixed in which both translation and rotation are constrained, were applied at the top of the piled raft. In addition to these simulations, a piled raft load test (*L*) was conducted numerically in to obtain the ultimate capacity of

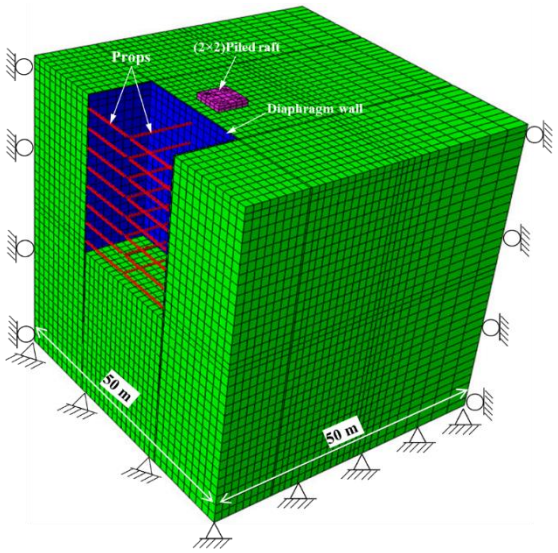

Fig. 3 3D finite element mesh of case H_e/L_p = 1.33 (showing model of piled raft, diaphragm wall and props)

the piled raft in sand. In total, 19 numerical simulations were performed to investigate ground and piled raft responses due to adjacent basement excavation, as summarized in Table 1. The finite element program Abaqus 6.10 (Hibbitt *et al*. 2010) was used to conduct numerical simulations.

2.2 Finite element mesh and boundary conditions

The finite element mesh, consisting of piled raft and the soil (incorporating excavation along with diaphragm wall and props), was generated using Abaqus CAE. Fig. 3 shows an isometric view of a typical finite element mesh in case of H_e/L_p = 1.33. The depth from the ground surface to the base of the mesh was 50 m.

Eight-noded hexahedral brick elements were used to model the soil, piled raft and the diaphragm wall, while two-noded truss elements are adopted to model the props. In the analysis, the piled raft installation effect on in situ stress distribution of soil was not considered and hence the ‘‘wished-in-place pile’’ was modelled. Therefore, the behaviour of the pile may be quite close to a bored pile. The obtained computed results can be conservative with this assumption.

The sensitivity of the numerical results with respect to size of mesh was explored and it was found that without undermining stability of analysis, the optimum value 1.5 mm of elements was chosen. A relatively fine mesh was used near the excavation and the piled raft because large shear strains were expected and the mesh became coarser further away from the structures (Soomro *et al.* 2022c). The numerical test shows that further halving current mesh size can only lead to a change of computed results of no more than 0.2%. Roller and pin supports are applied to the vertical sides and the base of the mesh, respectively. Therefore, movements normal to the vertical boundaries and in all directions of the base are restrained. The excavation-induced stress release process was modelled by the “element removal” technique which is widely used in finite element analysis. In this technique, the excavation process was simulated by deactivating soil elements inside excavation zone. In the meantime, the truss elements representing the props were activated.

The pile-soil and wall-soil interface is modelled as zero thickness by using duplicate nodes. The interface is modelled by the Coulomb friction law, in which the interface friction coefficient (μ) and limiting displacement (γ_{lim}) are required as input parameters. A limiting shear displacement of 5 mm is assumed to achieve full mobilization of the interface friction equal to μ×p', where p' is the normal effective stress between two contact surfaces and a typical value of μ for a bored pile of 0.35 is used in all analyses. This was based on relevant case histories reported by Francescon (1993) and Lee and Ng (2007). The excavation process will be simulated by deactivating soil elements inside excavation zone. In the meantime, the truss elements representing the props will be activated.

2.3 Constitutive model and model parameters used in finite element analyse

Since the stress-strain relationship of soils is highly nonlinear even at very small strain and the stiffness of soil depends on the recent stress or strain history of the soil (Atkinson *et al*. 1990, Hong *et al*. 2017), an advanced hypoplastic model was used to simulate the behaviour of sand in this study. The reason to adopt this model is because it is capable to reasonably excavation-induced ground deformations in sand, as reported by Soomro *et al.* (2021a, b, c).

The hypoplastic model was developed to describe non-linear response of granular material (Gudehus 1996, Herle and Mašín 1999) It consists of eight model parameters (ϕ'_c, h_s, n, e_{d0}, e_{c0}, e_{i0}, a and β). The first six parameters (ϕ'_c, h_s, n, e_{d0}, e_{c0}, e_{i0}) of Toyoura sand were calibrated by Herle and Gudehus (1999). The remaining two parameters (a and b) were obtained by curving fitting Maeda and Miura (1999) triaxial test results (at large strains). To account for strain-

Table 2 Hypoplastic model parameters of sand adopted in this study

Description	Parameter
Effective angle of shearing resistance at critical state: $\phi_c^{'}$	31°
Hardness of granulates, h_s	2.6 GPa
Exponent n	0.27
Minimum void ratio at zero pressure, e_{d0}	0.61
Maximum void ratio at zero pressure, e_{c0}	1.10
Critical void ratio at zero pressure, e_{i0}	0.98
Exponent α	0.14
Exponent β	6
Parameter controlling initial shear modulus upon 180° strain path reversal, m_R	11
Parameter controlling initial shear modulus upon 90° strain path reversal, m_T	6
Size of elastic range, R	2×10^{-5}
Parameter controlling degradation rate of stiffness with strain β_r	0.1
Parameter controlling degradation rate of stiffness with strain χ	1.0

Table 3 Concrete parameters adopted in finite element analysis

Description	Parameter
Young's Modulus, E	35 GPa
Poisson's ratio, ν	0.3
Density, ρ	2400 kg/m^3

dependency and path-dependency of soil stiffness (at small strains), Niemunis and Herle (1997) further improved the hypoplastic model by incorporating intergranular strain concept into the model. Five additional parameters (m_R, m_T, R, β_r and χ) are required. These five parameters were obtained by curve fitting stiffness degradation curves of Toyoura sand measured in this study. The coefficient of at-rest earth pressure (K_0=0.5) was estimated based on effective angle of shearing resistance at critical state ($\phi_c^{'}$=31°, as reported by Ishihara, 1993) and Jáky (1944)'s equation. Table 2 summarises model parameters of Toyoura sand adopted in the numerical analyses.

The concrete pile, the diaphragm wall and the props were assumed to be linear elastic with Young's modulus of 35 GPa and Poisson's ratio of 0.25. The unit weight of concrete was assumed to be 24 kN/m^3. The parameters for the piles and the diaphragm wall are summarised in Table 3.

2.4 Numerical modelling procedure

The numerical analysis modelling procedure for a typical case (i.e., H_e/L_p = 0.67) is summarized as follows:

a) Step 1: Set up the initial boundary and initial stress conditions (i.e., static stress conditions with K_o=0.5)
b) Step 2: Activate the brick elements representing piled raft (modelled as "wished-in-place").
c) Step 3: Apply the working load (determined from numerical pile load test) on the piled raft.
d) Step 4: Activate the brick elements representing the diaphragm wall.
e) Step 5: Staged multi-propped excavation is simulated as described in section 2.1. After excavating to 3 m depth, the first level of props is installed at 1 m below the ground surface.
f) Step 6: Repeat step 5 to excavate the next stages and install props until the last stage of excavation (i.e., H_e=12 m) is completed.

3. Interpretation of computed results

3.1 Determination of working load for the piled raft

This parametric study aims at investigating responses of the piled raft subjected to a working load due to adjacent excavations with different formation level relative to the pile length in sand. A numerical load test was carried out to compute ultimate load carrying capacity of the piled raft. The load of 3 MN (with increment of 1 MN) was applied on the pile over period of 24 hours. Fig. 4 shows load-settlement curve obtained from numerical load test. Based on the failure criterion, suggested by ISSMFE (1985) (i.e., 10% of pile diameter), the ultimate bearing capacity of 40.3 MN was computed. Using factor of safety as 3 (Poulos 2001), the working load was determined to be 16.13 MN. The settlement of the piled raft was 8.0 mm (1.0%d_p) due to application of the working load.

3.2 Effects of excavation depths

3.2.1 Induced settlement of the piled raft due to different excavation depths

Fig. 5 illustrates the normalised incremental settlement of the piled raft (S_p/d_p) with different excavation depths systems (i.e., H_e/L_p = 0.67, H_e/L_p = 1.00 and H_e/L_p = 1.33). Excavation depths are indicated by h. The piled settlement is normalised by pile diameter (d_p). For comparison, measured settlement of a single pile (diameter of pile = 0.8 m with embedded length= 20 m in prototype) due to

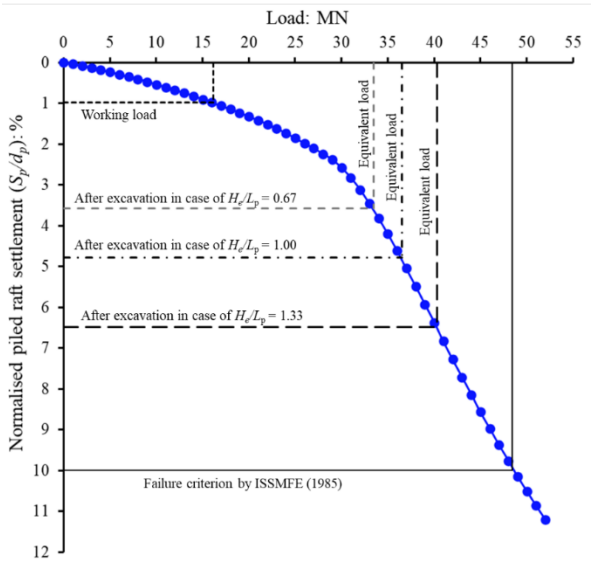

Fig. 4 Computed load settlement curve from the piled raft load test without excavation

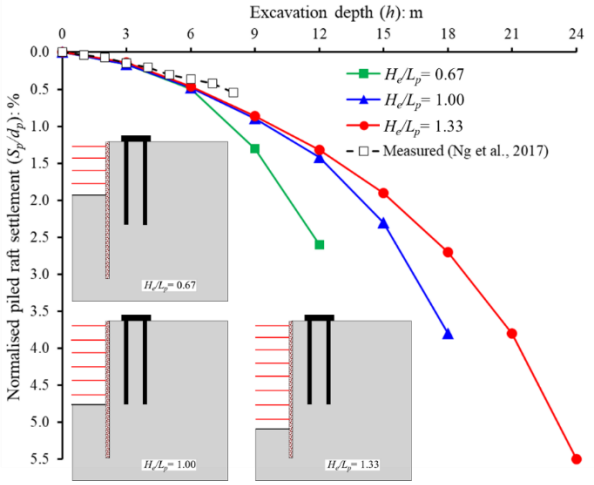

Fig. 5 Induced settlemnt of the piled raft during excavation

multipropped excavation in dry sand measured in centrifuge test (by Ng *et al.* 2017) is also included. It can be seen from the figure that non-linear increment in S_p was observed with increasing excavation depth in each case. The S_p increased linearly with excavation depth, however, rate of induced settlement increased during last two excavation stages (i.e., 6-12 m, 12-18 m and 18-24 m in case of H_e/L_p = 0.67, H_e/L_p = 1.00 and H_e/L_p = 1.33, respectively).

This is because of degradation of stiffness of sand due to excavation-induced stress release and shear strain surrounding the pile. As shown in figure similar characteristics of excavation-induced settlement of single pile was observed from the centrifuge test reported by Ng et al., 2017. However, the final measured induced settlement of single pile is smaller than that of piled raft. This can be attributed to the working load and excavation depth. The working load applied on the single pile is smaller than that on the piled raft and final depth of adjacent excavation is only 9 m.

By making comparison of induced settlement of the piled raft in case of H_e/L_p = 0.67 and H_e/L_p = 1.00, it is observed that the S_p during last two excavation stages (i.e., 9-12 m) in former case is larger than that of due to corresponding excavation stages in later case. To be more specific, larger settlement induced in case of H_e/L_p = 0.67 than that of in case of the H_e/L_p = 1.00 due to same stress release due to due to excavation stages (9-12 m). The additional amounts of induced-settlement at excavation depth of 9 m and 12 m are $0.44d_p$% and $1.18d_p$%, respectively. Similarly, the S_p induced during excavation stages (12-18 m) in case of H_e/L_p = 1.00 is higher than of in case of H_e/L_p = 1.33. This can be ascribed to different embedded depths of the diaphragm wall in each case. The computed results in this study have revealed that the induced settlement of the piled foundation depends upon the embedded depth of the diaphragm wall, type of pile foundation and applied working load on the pile. Among the three cases discussed, the largest and smallest settlement induced in the pile is in case of H_e/L_p = 1.33 and H_e/L_p = 0.67. This is because the piled raft is subjected to higher stress release due to excavation in case of H_e/L_p = 1.33 than that due to excavation in case of H_e/L_p = 0.67 and the entire

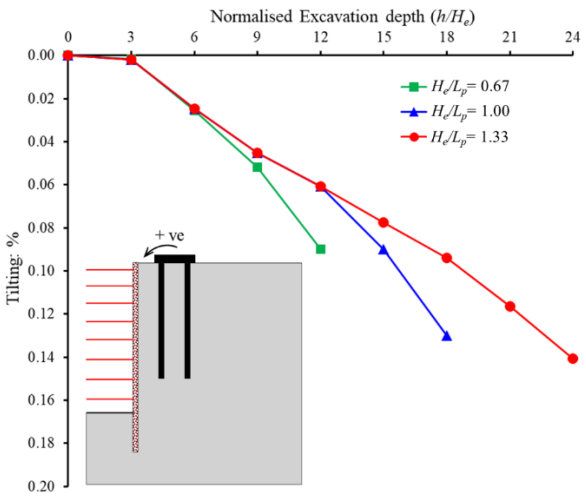

Fig. 6 Induced tilting of the raft during excavation

pile is located within the zone of excavation-induced displacement in case of H_e/L_p = 1.33 (discussed in section 3.3.3).

The piled raft experienced total settlements (due to working-load and excavation) of 29, 39 and 52 mm (i.e., 3.6, 4.8 and 6.5% of pile diameter) in case of H_e/L_p=0.67, H_e/L_p = 1.00 and H_e/L_p=1.33, respectively. Zhang and Ng (2005) proposed a reliability-based serviceability criterion for settlement (i.e., 56 mm), based on information from 95 settling buildings. Based on their criterion, after excavation in case of H_e/L_p=1.33, the pile violates the serviceability requirement.

3.2.2 Apparent loss of load carrying capacity of piled raft due to excavation

It is well-known that the load carrying capacity of a piled foundation is determined using displacement-based failure criterion. Therefore, additional settlement of the piled raft due to excavation can be estimated as apparent loss of load carrying capacity of the piled raft (ALPC). The settlement of the piled raft after application of working load of 16.13 MN (but before excavation) was 8 mm (0.98%d_p). The piled raft experienced an additional settlement of 21 mm (2.6%d_p) due to excavation in case of H_e/L_p=0.67. With this additional settlement (i.e., 3.6%d_p), the piled raft behaves as if it were loaded by a load of 33.5 MN (deduced from the load settlement curve shown in Fig. 4). Thus, the increase in equivalent load due to the excavation can be calculated to be 17.44 MN (= 33.5 - 16.1 MN). The additional load accounts for 36% of the ultimate capacity of the raft (i.e., 48.4 MN as shown in Fig. 4). In other words, an apparent loss of piled raft capacity (ALPC) of 36% was resulted due to the adjacent excavation in case of H_e/L_p=0.67. Similarly, ALPC can be readily calculated in cases of H_e/L_p = 1.00 and H_e/L_p = 1.33 as 42% and 50%, respectively.

3.2.3 Induced tilting of the raft due to different excavation depths

To support the high-rising buildings, the piled raft is preferred to the elevated pile group because the raft connected with piles contributes to avoiding differential settlement in the building and enhances the load-carrying capacity of the foundation (Bhaduri and Choudhury 2021, Poulos 2001). However, if the excavation is carried out the piled raft, it is likely that differential settlement can be induced in the raft. Hence, it is necessary to understand the tilting mechanism of the piled raft during the excavation. The differential settlement is presented in terms of tilting which is defined as the ratio of the differences in settlement between the two edges of the piled raft and the distance between the edges. Tilting toward the excavation is taken as positive and away from the excavation as negative.

Fig. 6 shows induced tilting of the piled raft due at different excavation depths systems (i.e., H_e/L_p = 0.67, H_e/L_p = 1.00 and H_e/L_p = 1.33). It can be observed from the figure that the tilting increased non-linearly during excavation in all the three cases (i.e., H_e/L_p = 0.67, H_e/L_p = 1.00 and H_e/L_p = 1.33).

The rate of induced tilting increased during last two excavation stages (i.e., 6-12 m, 12-18 m and 18-24 m in cases of H_e/L_p = 0.67, H_e/L_p = 1.00 and H_e/L_p = 1.33, respectively). Since the excavation was carried out on one side of the piled raft, the non-uniform stress release induced around the piled raft. The row of piles nearest the excavation (i.e., front row) is subjected to higher stress release than that of farthest the excavation (i.e., rear row). Consequently, the front row piles settled larger than that of the rear row due to excavation which caused differential settlement in the piled. Similar to the induced settlement chrematistics, S_p during last two excavation stages (i.e., 9-12 m) in case of H_e/L_p = 0.67 is larger than that of due to corresponding excavation stages in case of H_e/L_p = 1.00. To be more specific, larger tilting induced in case of H_e/L_p = 0.67 than that of in case of the H_e/L_p = 1.00 due to same stress release due to excavation stages (9-12 m). The additional amounts of induced-tilting at excavation depth of 9 m and 12 m are 0.007% and 0.03%, respectively. Similarly, the tilting induced during excavation stages (12-18 m) in case of H_e/L_p = 1.00 is higher than of in case of H_e/L_p = 1.33. This can be ascribed to different embedded depths of the diaphragm wall in each case. Among the three

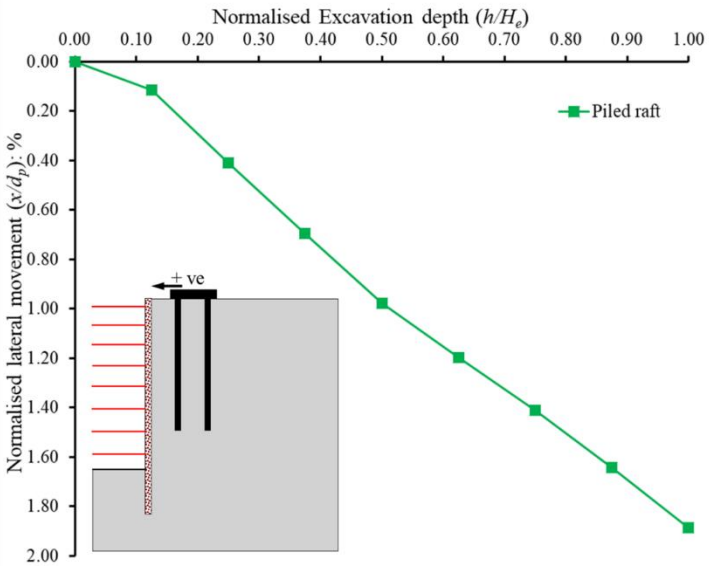

Fig. 7 Induced lateral movment of the raft during excavation

cases discussed, the largest and smallest tilting induced in the raft is in case of H_e/L_p = 1.33 and H_e/L_p = 0.67. This is because the piled raft is subjected to higher stress release due to excavation in case of H_e/L_p = 1.33 than that due to excavation in case of H_e/L_p = 0.67 and the entire pile is located within the zone of excavation-induced displacement in case of H_e/L_p = 1.33 (discussed in section 3.3.3). On completion of the excavation, the amount of tiling was is 0.09, 0.13, and 0.14% in cases of H_e/L_p = 0.67, H_e/L_p = 1.00 and H_e/L_p = 1.33, respectively.

To prevent the occurrence of a serviceability limit state in structures, the maximum acceptable tilting is given by Eurocode 7 (2004) for different types of structures. For open framed structures, infilled frames and load bearing or continuous brick walls, the allowable limit of tilting is in a wide range of 1/2000 to 1/300. In practice, a maximum tilting of 1/500 is widely chosen for many structures. Zhang and Ng (2005) proposed reliability-based limiting tolerable value of tilting (i.e., 0.25%) established on 57 cases of deep foundation. Since structure type is not considered in this study, a typical allowable limit of 1/500 (i.e., 0.20%) is thus used for comparison purpose. Based on the configuration of the geometry, ground conditions, and the excavation depths, the induced tilting in each case does not exceed the limit values recommended by Zhang and Ng (2005) and Eurocode 7 (2001).

3.2.4 Induced lateral movement of the raft due to different excavation depths

As discussed earlier, the piled raft is subjected to stress release on one side of the piled raft. Therefore, the excavation caused not only differential settlement (tilting) but also lateral movement of the raft in the direction of the excavation. Fig. 7 illustrates the induced lateral movement of the raft (x) due to excavation at different stages of excavation.

Lateral movement toward the excavation is taken as positive and away from the excavation as negative. It can be seen that the induced lateral movement of the raft increased linearly with excavation stages except during first excavation stage. This is because of two reasons. Firstly, the piled raft is subjected to larger shear strain due to excavation-induced stress release as the excavation depth increases. Second reason is the degradation of stiffness of sand with strain due to excavation-induced stress release. In this study, the ground (sand) is modelled using an advanced constitutive soil model (i.e., hypoplastic model) which is capable to capture small-strain stiffness. The deeper excavation depth induced large shear strain causing significant of stiffness degradation near the diaphragm wall. The final lateral movement of the raft was 15 mm (i.e., 1.88% pile diameter). This conclusion might not be applicable to scenarios in which the ground conditions are different from those adopted in this study.

3.2.5 Induced pile lateral displacement due to different excavation depths

In this section, the lateral displacement of a typical pile P1 (closest to the excavation) is selected for discussion in each case (H_e/L_p = 0.67, H_e/L_p = 1.00 and H_e/L_p = 1.33). Fig. 8 shows the pile deflection profile along the depth of the pile P1 in each case. It can be seen from the figure that as excavation was carried out, the pile deflected towards excavation in all the three cases.

This is because of excavation-induced effective stress release and soil displacement towards excavation. When the first stage was excavated, the upper part of the pile deflected more than the lower part of the pile. As excavation proceeds, significant lateral displacement was induced in lower part of the pile. In contrast, the upper part of the pile (i.e., near the head) displaced away from the excavation. The substantial lateral displacement of the lower part of the pile is due to further effective stress-release and soil movement during excavation. adjacent excavation of the pile was observed by Liyanapathirana and Nishanthan (2016). On completion of excavation in cases of

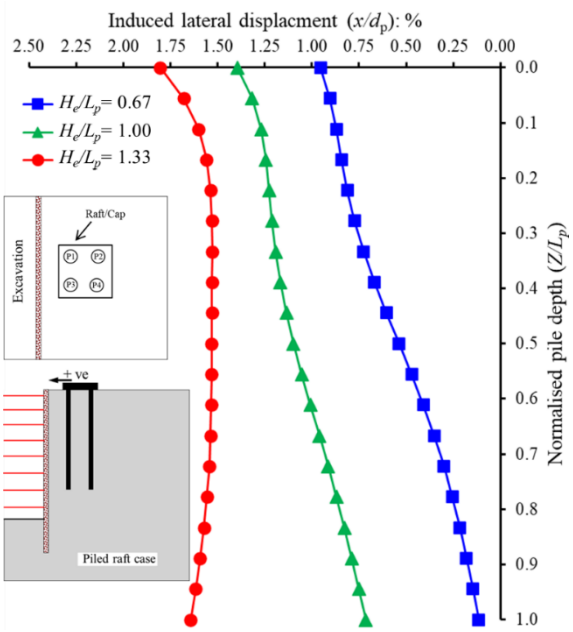

Fig. 8 Induced lateral deflection of pile P1

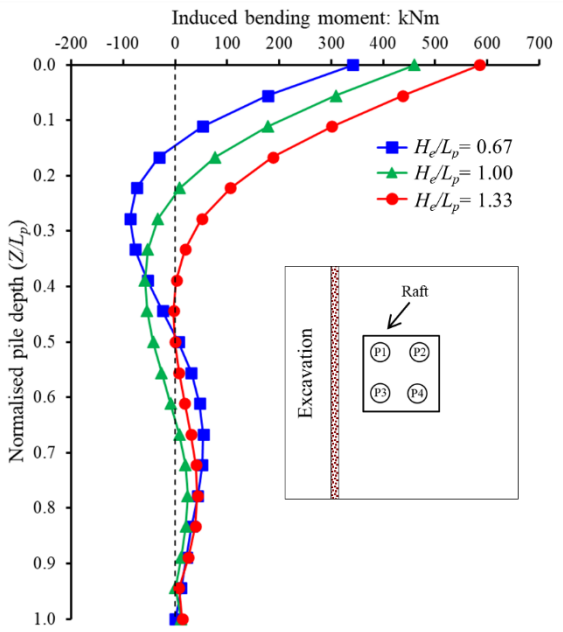

Fig. 9 Induced bending moment in pile P1

H_e/L_p=0.67, 1.00 and 1.33, the maximum deflection of 8.0 mm (1.0%d_p), 11.2 mm (1.4%d_p) and 14.4 mm (1.8%d_p), respectively.

3.2.6 Excavation-induced bending moment in the pile

As discussed in section 3.2.3, the tilting was induced in the piled raft due to stress-induced excavation. As a result of tilting, bending moment was induced at/near piles head in the piled raft during excavation. Fig. 9 illustrates bending moment profile in pile on completion of excavation in all three cases (i.e., H_e/L_p = 0.67, H_e/L_p = 1.00 and H_e/L_p = 1.33).

The induced-bending moment is taken as positive if compressive stress was induced along the pile shaft facing the excavation. It can be observed that the induced bending moment along the length of pile P1 increases as excavation depth increases. Moreover, substantial positive bending moment was induced at/near the head of the pile in each case. This is because the induced tilting of the piled raft and lateral movement of the pile is restrained due to rigid connection with the pile cap. To counter-balance the positive moment at the pile head, a negative bending moment was induced in the pile. This is attributed to lateral soil movement towards excavation as a result of stress release. The maximum positive bending moment was 200 kNm at Z/L_p=0.67. Since pile toes are free to move, no any bending moment was induced in both the piles at the toes. It is observed that as excavation stages proceeds, the induced

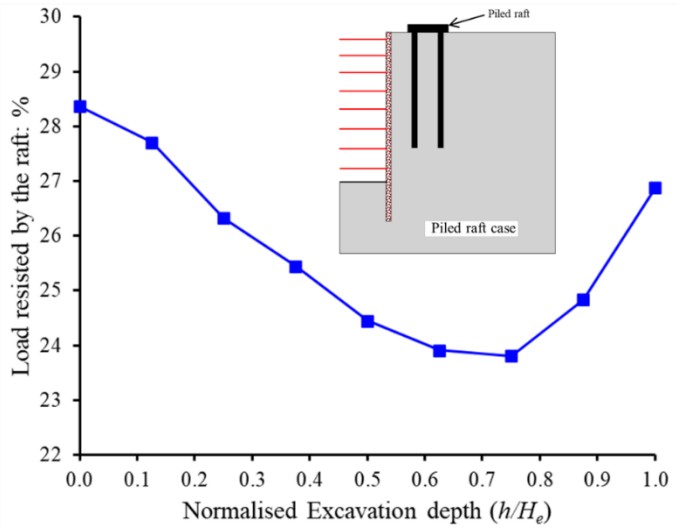

Fig. 10 Changes in load resisted by the raft during excavation

bending moment varies along the length of pile. The maximum bending moments of 585, 460 and 342 kNm were induced at the pile head due to excavation in cases of H_e/L_p = 0.67, H_e/L_p = 1.00 and H_e/L_p = 1.33, respectively.

It can be seen that the maximum induced bending moment at the end of excavation in all the three cases is less than the pile bending moment capacity (i.e., 800 kNm). Therefore, the most critical issue to be considered in excavation-soil-pile problem is relatively large settlement and lateral displacement of the pile. This conclusion may not be applicable to scenarios in which the ground conditions or stiffness of excavation system (i.e., wall and prop stiffness) are different from those adopted in this study.

3.2.7 Changes in piled raft load transfer mechanism due to excavation

After the application of the working load on the top of the piled raft, some load is taken by the raft, and the remainder of the load is transferred to the piles. The piled raft supports the load by mobilizing stresses in the ground (Lu *et al*. 2020, Soomro *et al*. 2022b). Since the process of the excavation essentially induced stress release in the ground, load redistribution occurs between the raft and the piles. Fig. 10 shows the change in load sharing by the raft during excavation. It can be seen that before excavation (after application of working load), about 28% of the working load (i.e., 16.13 MN) was carried by the raft and rest of the load was transferred to the four piles equally. It can be seen from the figure that the load taken by the raft kept decreasing till excavation reaches at two-third of excavation depth (h/H_e=0.75). This suggested that some of the working load was transferred to the four piles and the piled raft system behaves as elevated pile group (in which the pile cap is raised above the ground) after excavation. This can be attributed to separation of the raft and the ground because of induced larger ground surface settlement and lesser piled raft settlement. As a result of the gap between the raft and the piles, the effective vertical stress decreased significantly on completion of the excavation. However, as excavation proceeds beyond h/H_e=0.75, the load taken by the raft kept increasing till completion of the excavation. This implies that the load is re-transferred to the raft. This is because the deeper excavation led to substantial settlement in the raft but less ground surface settlement. The load carried by the raft reduced to 5% at excavation stage h/H_e=0.75 and after that increased to 3% on completion of the excavation.

3.2.8 Load redistributions among piles in piled raft due to excavation

As discussed in previous section that the changes occurred in the load resisted by the raft during excavation. Therefore, load redistribution also occurred among piles in the piled raft. Fig. 11 shows the changes in head load (p) of piles P1, P2, P3 and P4 during excavation.

The change in the pile head load (Δp) is normalised by the load taken by each pile (p_i) before the excavation. Since excavation was carried out at one side of the excavation (see inset in the figure), the changes in the head loads of the pile closest to the excavation (piles P1 and P3) and the changes in the head loads of the pile farthest to the excavation (piles P2 and P4) are same during excavation. It can be seen from the figure that the head load of all four piles increase as excavation depth reaches at half of final excavation depth (h/H_e=0.5). This is because the load resisted by the raft decreases (see Fig. 10). Consequently, load transferred to the piles resulting in increment of pile head loads. However, as the excavation further proceeds the load at the heads of piles P1 and P3 decreased significantly. This is because of excavation-induce stress release and soil movement towards excavation led to reduction of shaft resistance along the pile.

To support the constant working load acting on the raft, the head load of pile P2 as well as that of pile P4 and the load taken by the raft increased as a result of load redistribution from piles P1 and P3. Owing to load redistribution among piles during excavation, the rear piles (i.e., P2 and P4) experienced the most significant increase of 12% in head load.

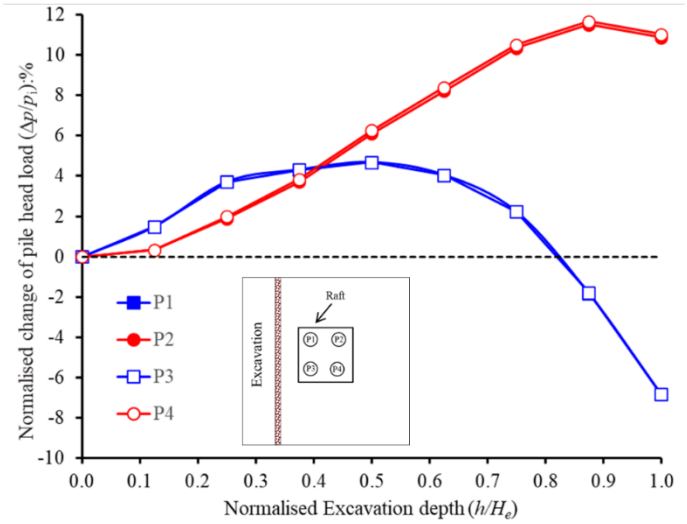

Fig. 11 Load-redistributions among piles in the piled raft during excavation

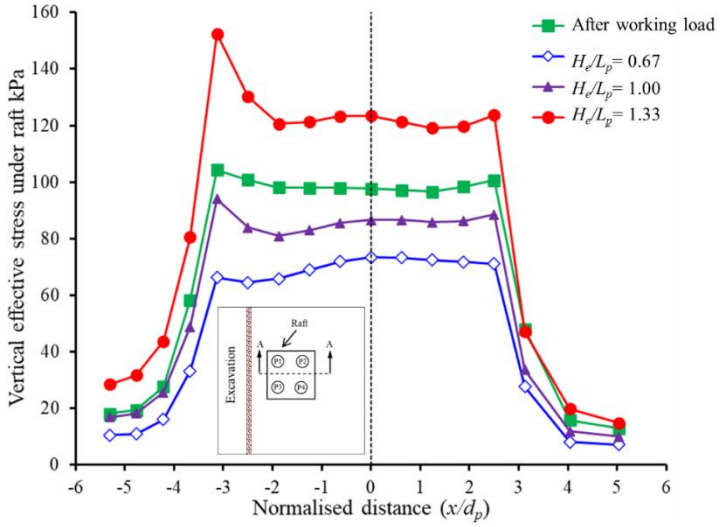

Fig. 12 Changes in vertical effective stress (σ'_v) in the ground immediately below the raft

3.2.9 Changes in pressure in the ground underneath the raft

The raft supports the applied working load by generating stresses in the soil. On the contrary, excavation is essentially a stress-release process in the ground. Therefore, it is worth investigating the pressure changes underneath the raft during excavation to understand the load transfer in the piled raft. Fig. 12 shows the changes in pressure (i.e., vertical effective stress) in the ground beneath the raft due to excavation in all three cases (i.e., H_e/L_p = 0.67, H_e/L_p = 1.00 and H_e/L_p = 1.33). The pressure underneath the raft reduced significantly after the completion of the excavation in case of H_e/L_p = 0.67.

This is because of stress release due to excavation resulted in the transfer of load taken by the raft to the pile heads. The ground pressure decreased by 38 kPa underneath the raft excavation. As the excavation goes deeper in cases of H_e/L_p = 1.00 and H_e/L_p = 1.33, the pressure in the ground underneath the raft increased. The reason is ascribed to large raft settlement due to excavation in both the cases (H_e/L_p = 1.00 and H_e/L_p = 1.33) as compared to that in case of H_e/L_p = 0.67. As compared to the ground surface settlement in cases H_e/L_p = 1.00 and H_e/L_p = 1.33, large settlement of the raft induced due to excavation, which caused penetration of the raft into the ground resulting in the increment of the ground pressure. Consequently, the load carried by the raft increased substantially (see Fig. 10). The ground pressure increased by 50 kPa underneath the raft excavation in the case of H_e/L_p = 1.33.

3.3 Effects of sand density

3.3.1 Induced piled raft settlement

Fig. 13 shows the induced settlement of the piled raft constructed in sand with different relative density (i.e., D_r =30%, 50%, 70% and 90%) due to excavation at different depths (i.e., h/H_e = 0.2, 0.44, 0.56, 0.8 and 1.0). It can be seen that the induced settlement increases linearly with excavation depths in the sand with different relative density. However, piled raft settlement decreases with increasing sand relative density. On completion of the excavation (h/H_e=1.0), the induced piled raft settlement in loose sand

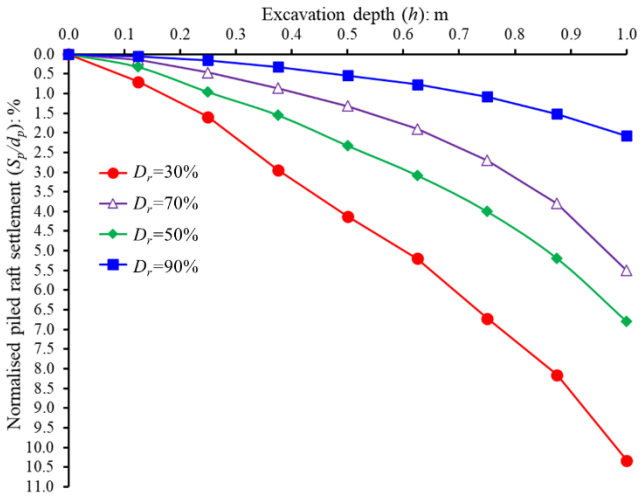

Fig. 13 Effect of sand density on settlement of the raft due to excavation

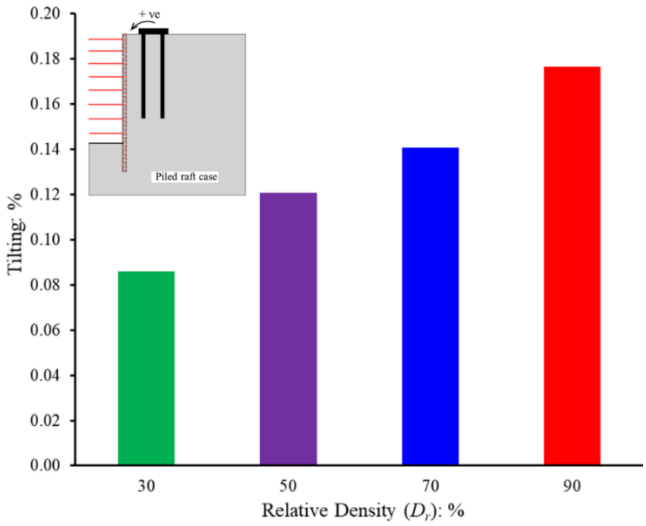

Fig. 14 Effect of sand density on the raft tilting due to excavation

(D_r=30%) and dense sand (D_r =90%) are 10.3d_p% and 2.07d_p%, respectively. The settlement of the footing was reduced by 80%. This is because loose sand has a smaller stiffness than that of dense sand. Due to excavation-induced stress relief, large soil movements are induced in loose sand (discussed in section 3.3.3), causing larger footing settlement. Since shallow excavations induce smaller stress relief, the effects of the relative density of sand on piled raft settlement is less significant than that of deep excavations.

3.3.2 Induced tilting of the raft

As discussed in previous section, the sand density effects the induced settlement of the piled raft due to excavation significantly. Hence, it is necessary to investigate the ground density effects on induced tilting of the raft. Fig. 14 shows the indued tilting of raft in the sand with different relative density (i.e., D_r =30%, 50%, 70% and 90%) on completion of excavation. Unlike induced settlement of the piled raft, the induced tilting of the raft increases almost linearly with increasing density of sand. This is because of the ground movement and shear strain induced due to excavation. In loose sand (D_r =30%), the zone of the ground movement and shear strain due to excavation is larger and wider than that of in dense sand (discussed in section 3.3.3). The row of piles closets to the excavation in dense sand is severely affected as compared to that of farthest to the excavation. A smaller amount of tilting (0.08%) therefore resulted in the loose sand test than in dense sand (0.17%).

3.3.3 Ground soil movements

Fig. 15(a)-15(d) show the soil movement on completion of excavation in the ground with different sand densities of D_r = 30%, 50%, 70% and 90%, respectively. In addition, excavation-induced shear strain contours are also superimposed in each figure.

As it can be seen that soil behind the wall flows towards the excavation causing the pile to displace laterally in all the three cases. In each case the induced soil displacement is uniform along the entire pile. However, the heave in the formation level was induced at excavation side. The deep-seated horizontal soil movements indicate the “bulging”

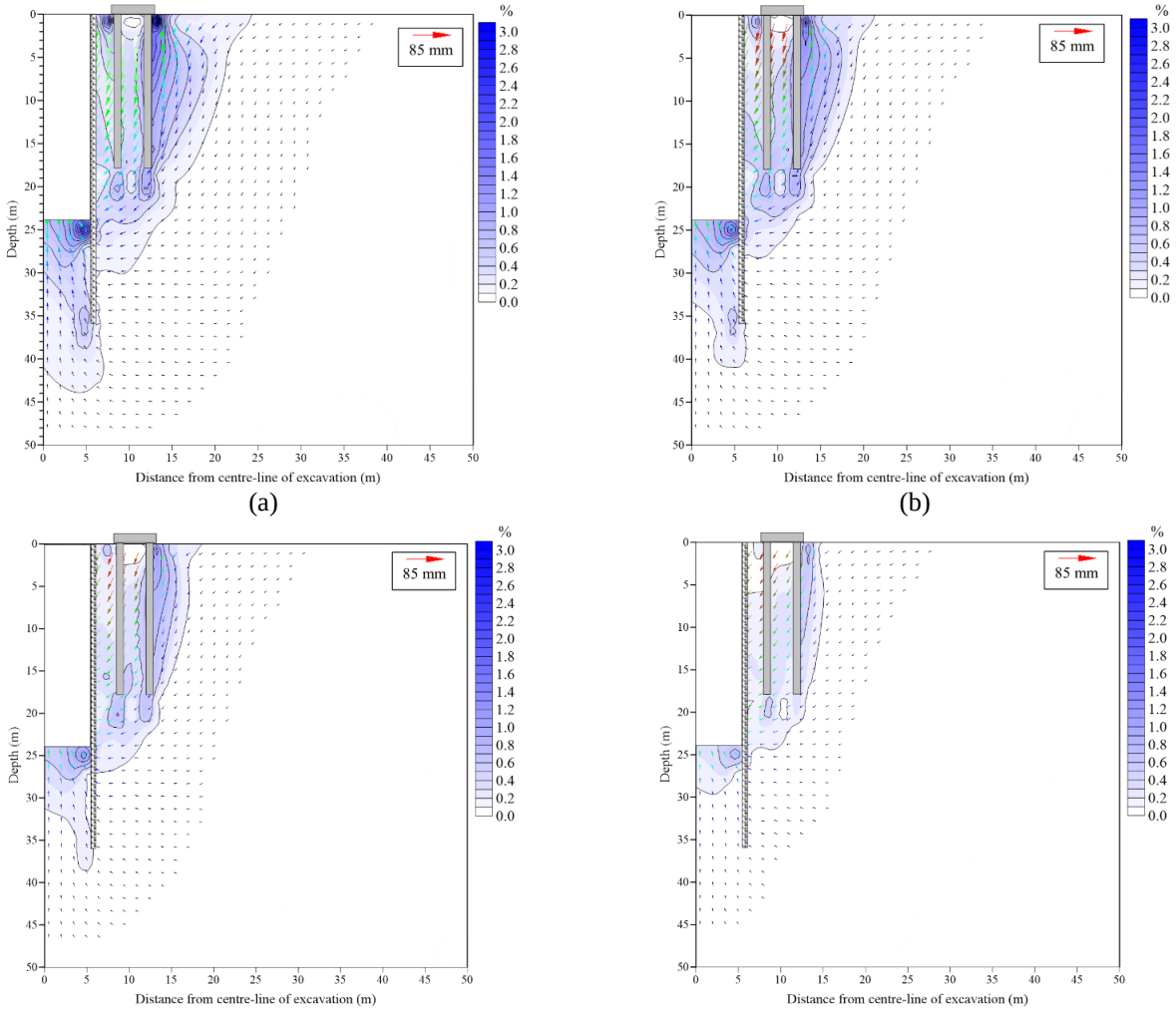

Fig. 15 Effects of the sand relative density on the induced soil movement and shear strain contours (a) D_r=30%, (b) D_r =50%, (c) D_r =70% and (d) D_r =90%

profiles of the wall deformation. The soil movement in loose ground (i.e., D_r=30%) is larger than that in denser grounds. This is because of lower shear modulus of loose sand. The horizontal influence zone is larger when the sand density is lower (ranging from 1.6 to 0.6H_e for D_r=30% and 90%, respectively). This caused the larger tilting of the piled raft in dense sand that that in loose sand. As the relative sand density increases from 30% to 90%, the maximum soil movement decreases from 80 mm to 20 mm. It implies that when the sand density decreases, the reduction of soil stiffness dominates the soil movements rather than stress relief. The larger soil movement in loose sand caused larger piled raft settlement (see Fig. 13) due to excavation.

3.4 Effects of raft fixity

3.4.1 Induced lateral displacement along pile length

Fig. 16 compares induced lateral displacement of the pile with different raft conditions (i.e., free, pinned and fixed) on completion of excavation, respectively. The pile deflection toward the excavation is regarded as positive.

It can be seen from the figure that the pile lateral displacement in case of pinned and fixed raft conditions was observed to zero at the ground surface, as expected. Moreover, the induced-pile deflection profiles are similar along the pile length in cases of pinned and fixed raft conditions. During the excavation, the pile deflection increased along the depth with maximum value at pile toe. In case of free raft condition, the pile moved as a rigid cylindrical body. On the contrary, the raft with pinned and fixed condition, the lower part of the piled raft displaced laterally towards the excavation. Consequently, the induced bending moment and shear force along the pile length in case of free raft condition is smaller than that in cases of the raft with pinned and fixed condition.

3.4.2 Induced bending moment along pile

Fig. 17 illustrates the comparison between induced bending moment profile in the pile with different raft conditions (i.e., free, pinned and fixed) on completion of excavation. The induced-bending moment is taken as positive if tensile fibre faces towards excavation.

It can be seen that the induced bending moment profiles

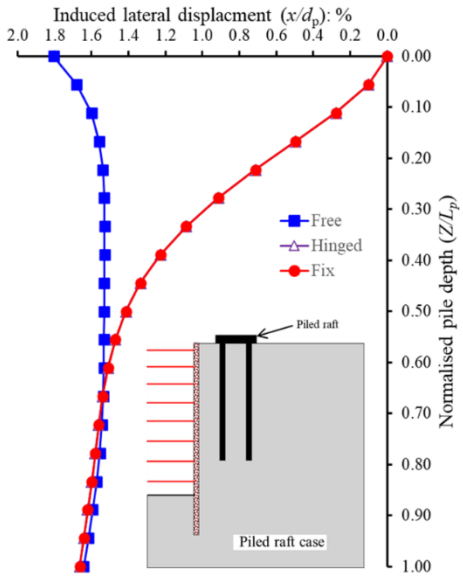

Fig. 16 Effect of the raft fixity on induced pile deflection due to excavation

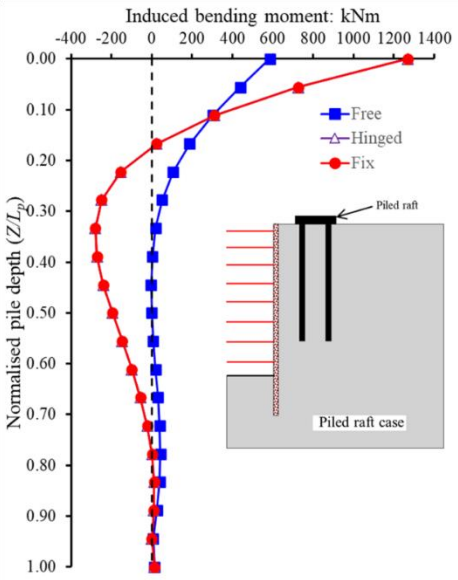

Fig. 17 Effect of the raft fixity on induced bending moment in pile due to excavation

in the pile with retrained head conditions are quite different from that in free pile head condition in all the cases. Due to head constraint higher negative bending moment was induced at pile head in all the three cases. As excavation depth increase positive bending moment is induced at lower portion of the pile in constraint head conditions. In contrast only positive bending moment is induced in the free head pile. The negative bending moment at pile head in constrained conditions increases as excavation depth increases. The maximum negative bending moment of 375, 430 and 480 kNm at the pile head was induced in case of H_e/L_p = 0.67, H_e/L_p = 1.00 and H_e/L_p = 1.33, respectively.

3.4.3 Induced lateral force along pile

Fig. 18 compares the induced lateral force along the piles with different raft conditions (i.e., free, pinned and fixed) on completion of excavation. The positive induced-shear force indicates the direction of the force towards the excavation.

It can be observed from the figure that the maximum lateral force induced at/near pile head in all the three different raft conditions. However, the lateral force decreases along the length of the pile and becomes zero at the pile toe. This is because the pile head in constraint with raft and pile is free to move. The induced ground movement is towards excavation. The inward soil movement tends to push the pile towards the excavation. Consequently, the lateral forces are developed in opposite direction of that of the first tunnel. To counterbalance the negative induced lateral force, positive lateral force was induced at the lower portion (i.e., $Z/L_p \geq 0.30$). The maximum value of 150 kN induced at pile head. Comparing the induced lateral force in free condition of raft, the induced lateral force in pile is larger in pinned and fixed raft condition. The reason can be

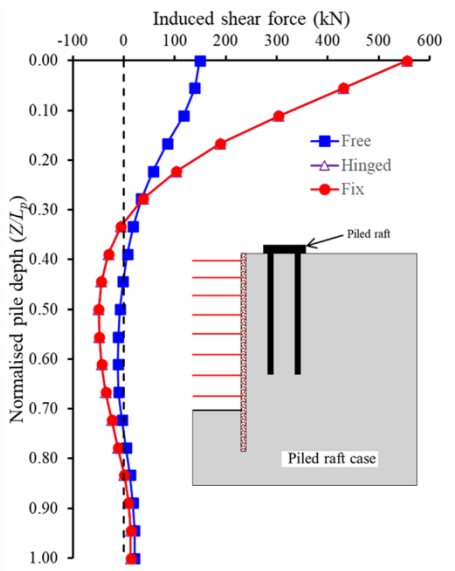

Fig. 18 Effect of the raft fixity on induced lateral force in pile due to excavation

ascribed to the fixity of the raft. The maximum lateral force of magnitude 560 kN was induced in pinned and fixed raft condition.

5. Conclusions

In this study, a parametric study was carried out to investigate the settlement and load transfer mechanism of a (2×2) piled raft due to different excavation depths systems in sand. The effects of excavation depths relative to pile were investigated by simulating the excavation near the pile shaft (i.e., H_e/L_p=0.67), next to (H_e/L_p = 1.00) and below the pile toe (H_e/L_p=1.33). In addition, the effects of different relative density (i.e., D_r = 30%, 50%, 70% and 90%) and different raft fixity condition (i.e., free, pinned and fixed) on the responses to the piled raft due to excavation were investigated.

a) The response of the piled raft due to excavation in case of H_e/L_p = 0.67 and H_e/L_p = 1.00 have revealed that the induced settlement, tilting, pile lateral movement and load transfer mechanism depends upon the embedded depth of the diaphragm wall.
b) Among the three cases discussed, the largest and smallest induced settlement and tilting in the piled raft was found in case of H_e/L_p = 1.33 and H_e/L_p = 0.67. This is because the piled raft is subjected to higher stress release due to excavation in case of H_e/L_p = 1.33 than that due to excavation in case of H_e/L_p = 0.67 and the entire piled raft is located within the zone of excavation-induced displacement in case of H_e/L_p = 1.33.
c) Additional settlement of the piled raft due to excavation can be account for apparent loss of load carrying capacity of the piled raft (ALPC). The highest ALPC of 50% was calculated in in case of H_e/L_p = 1.33.
d) During the first stages of the excavation, load taken by the raft decrease significantly resulting in the transfer of load to the piles. However, as excavation proceeds beyond h/H_e=0.75, the load taken by the raft kept increasing till completion of the excavation.
e) Relative density of the sand substantially effects on the induced settlement and tilting of the piled raft due to excavation. The induced settlement decreased with increasing the relative density from 30% to 90%. On the contrary, the tilting of the raft increases in denser ground.
f) The maximum bending moment was induced at the pile head in all raft fixity conditions. The larger bending moment and lateral force was induced at the piled heads in fixed and pinned raft condition.

It should be noted that the computed results reported should be treated with caution since they may be specific to the particular soil type and isolated piled raft adopted in this paper.

Acknowledgments

The authors would like to acknowledge the financial support provided by Mehran University of Engineering & Technology, Jamshoro, Sindh and Pakistan.

Conflicts of Interest

The authors declare that they have no conflicts of interest.

References

Atkinson, J.H., Richardson, D. and Stallebrass, S.E. (1990), "Effect of recent stress history on the stiffness of over consolidated soil", *Géotechnique*, **40**(4), 531-540. https://doi.org/10.1680/geot.1990.40.4.531.

Bai, X.D., Cheng, W.C. and Li, G. (2021), "A comparative study of different machine learning algorithms in predicting EPB

shield behaviour: a case study at the Xi'an metro, China", *Acta Geotechnica*, **16**(12), 4061-4080. https://doi.org/10.1007/s11440-021-01383-7.

CEN (2001), Eurocode 7 part 1: Geotechnical design: General rules, Final Draft prEN 1997-1. European Committeef or Standardization (CEN), Brussels.

Finno, R.J., Lawrence, S.A., Allawh, N.F. and Harahap, I.S. (1991), "Analysis of performance of pile groups adjacent to deep excavation", *J. Geotech. Eng*., **117**(6), 934-955. https://doi.org/10.1061/(ASCE)0733-9410(1991)117:6(934).

Francescon, M. (1983), "Model pile tests in clay: Stresses and displacements due to installation and axial loading", PhD thesis, Cambridge Univ., Cambridge, U.K.

Goh, A.T.C., Wong, K.S., Teh, C.I. and Wen, D. (2003), "Pile response adjacent to braced excavation", *J. Geotech. Geoenviron. Eng.*, **129**(4), 383-386. https://doi.org/10.1061/(ASCE)1090-0241(2003)129:4(383).

Gudehus, G. (1996), "A comprehensive constitutive equation for granular materials", *Soils Found.*, **36**(1), 1-12. https://doi.org/10.3208/sandf.36.1.

Herle, I. and Gudehus, G. (1999), "Determination of parameters of a hypoplastic constitutive model from properties of grain assemblies", *Mech. Cohesive-frictional Mater.: Int. J. Exper. Model. Comput. Mater. Struct*., **4**(5), 461-486. https://doi.org/10.1002/(sici)10991484(199909)4:5%3C461::aid-cfm71%3E3.0.co;2-p.

Hibbitt, D., Karlsson, B.I. and Sorensen, E.P. (2010), Abaqus user's manual, version 6.10.2. Hibbitt, Karlsson & Sorensen Inc;, Providence, RI, USA.

Hong, Y., Koo, C.H., Zhou, C., Ng, C.W. and Wang, L.Z. (2017), "Small strain path-dependent stiffness of Toyoura sand: Laboratory measurement and numerical implementation", *Int. J. Geomech*., **17**(1), 04016036. https://doi.org/10.1061/(asce)gm.1943-5622.0000664.

Hsiung, B.C.B. (2009), "A case study on the behaviour of a deep excavation in sand", *Comput. Geotech.*, **36**(4), 665-675. https://doi.org/10.1016/j.compgeo.2008.10.003.

Hu, W., Cheng, W.C., Wen, S. and Rahman, M.M. (2021), "Effects of chemical contamination on microscale structural characteristics of intact loess and resultant macroscale mechanical properties", *Catena*, **203**, 105361. https://doi.org/10.1016/j.catena.2021.105361.

Hu, W., Cheng, W.C., Wang, L. and Xue, Z.F. (2022), "Micro-structural characteristics deterioration of intact loess under acid and saline solutions and resultant macro-mechanical properties", *Soil Tillage Res.*, **220**, 105382. https://doi.org/10.1016/j.still.2022.105382.

Ishihara, K. (1993), "Liquefaction and flow failure during earthquakes", *Géotechnique*, **43**(3), 351-415. https://doi.org/10.1680/geot.1993.43.3.351

ISSMFE (1985), "Axial pile loading test – Part I: Static loading", *Geotech. Test. J.*, **8**(2), 79-80, https://doi.org/10.1520/GTJ10514J.

Jáky, J. (1944), The coefficient of earth pressure at rest", *J. Soc. Hungarian Arch. Eng*., 355-8 [in Hungarian].

Korff, M., Mair, R. and Van Tol, F.A.F. (2016), "Pile-soil interaction and settlement effects induced by deep excavations", *J. Geotech. Geoenviron. Eng*., **138**(7), 04016034. https://doi.org/10.1061/(ASCE)GT.1943-5606.0001434.

Liyanapathirana, D.S. and Nishanthan, R. (2016), "Influence of deep excavation induced ground movements on adjacent piles", *Tunn. Undergr. Sp. Tech.*, **52**, 168-181. https://doi.org/10.1016/j.tust.2015.11.019.

Lee, C.J. and Chiang, K.H. (2007), "Responses of single piles to tunnelling-induced soil movements in sandy ground", *Can. Geotech. J.*, **44**, 1224-1241. https://doi.org/10.1139/T07-050.

Lu, H., Shi, J., Ng, C.W.W. and Lv, Y. (2020), "Three-dimensional centrifuge modeling of the influence of side-by-side twin tunneling on a piled raft", *Tunn. Undergr. Sp. Tech*., **103**, 103486. https://doi.org/10.1016/j.tust.2020.103486.

Maeda, K. and Miura, K. (1999), "Relative density dependency of mechanical properties of sands", *Soils Found.*, **39**(1), 69-79. https://doi.org/10.3208/sandf.39.69.

Niemunis, A. and Herle, I. (1997), "Hypoplastic model for cohesionless soils with elastic strain range", *Mech. Cohesive-frictional Mater.: Int. J. Exper. Model. Comput. Mater. Struct*., **2**(4), 279-299. https://doi.org/10.1002/(SICI)1099-1484(199710)2:4<279::AID-CFM29>3.0.CO;2-8.

Ng, C.W., Wei, J., Poulos, H. and Liu, H. (2017), "Effects of multipropped excavation on an adjacent floating pile", *J. Geotech. Geoenviron. Eng.*, **143**(7), 04017021. https://doi.org/10.1061/(ASCE)GT.1943-5606.0001696.

Ng, C.W., Shakeel, M., Wei, J. and Lin, S. (2021), "Performance of existing piled raft and pile group due to adjacent multipropped excavation: 3D centrifuge and numerical modeling", *J. Geotech. Geoenviron. Eng.*, **147**(4), 04021012.

Ong, D.E., Leung, C.E. and Chow, Y.K. (2006), "Pile behavior due to excavation-induced soil movement in clay. I: Stable wall", *J. Geotech. Geoenviron. Eng.*, **132**(1), 36-44. https://doi.org/10.1061/(ASCE)1090-0241(2006)132:1(36).

Ong, D.E.L., Leung, C.F. and Chow, Y.K. (2009), "Behavior of pile groups subject to excavation-induced soil movement in very soft clay", *J. Geotech. Geoenviron. Eng*., **135**(10), 1462-1474. https://doi.org/10.1061/(ASCE)GT.1943-5606.0000095.

Poulos, H.G. (2001), "Piled raft foundations: design and applications", *Géotechnique*, **51**(2), 95-113. https://doi.org/10.1680/geot.2001.51.2.95.

Shi, J., Liu, G., Huang, P. and Ng, C.W.W. (2015), "Interaction between a large-scale triangular excavation and adjacent structures in Shanghai soft clay", *Tunn. Undergr. Sp. Tech*., **50**, 282-295. https://doi.org/10.1016/j.tust.2015.07.013.

Shi, J., Wei, J., Ng, C.W. and Lu, H. (2019), "Stress transfer mechanisms and settlement of a floating pile due to adjacent multi-propped deep excavation in dry sand", *Comput. Geotech*., **116**, 103216. https://doi.org/10.1016/j.compgeo.2019.103216.

Soomro, M.A., Mangnejo, D.A., Saand, A. and Hong, Y. (2021a), "Responses of a masonry façade to multi-propped deep excavation-induced ground deformations: 3D numerical parametric study", *Eur. J. Environ. Civil Eng.*, 1-29. https://doi.org/10.1080/19648189.2021.1926336.

Soomro, M.A., Mangnejo, D.A., Saand, A., Mangi, N. and Auchar Zardari, M. (2021b), "Influence of stress relief due to deep excavation on a brick masonry wall: 3D numerical predictions", *Eur. J. Environ. Civil Eng.*, 1-24. https://doi.org/10.1080/19648189.2021.2004450.

Soomro, M.A., Mangnejo, D.A., Saand, A. and Mangi, N. (2021c), "3D numerical analysis of a masonry façade subjected to excavation-induced ground deformation", *Int. J. Geotech. Eng.*, 1-13. https://doi.org/10.1080/19386362.2021.1937853.

Soomro, M.A., Saand, A., Mangi, N., Mangnejo, D.A., Karira, H., and Liu, K. (2021d), "Numerical modelling of effects of different multipropped excavation depths on adjacent single piles: comparison between floating and end-bearing pile responses", *Eur. J. Environ. Civil Eng.*, **25**(14), 2592-2622. https://doi.org/10.1080/19648189.2019.1638312.

Soomro, M.A., Mangi, N., Memon, A.H. and Mangnejo, D.A. (2022a), "Responses of high-rise building resting on piled raft to adjacent tunnel at different depths relative to piles", *Geomech. Eng.*, **29**(1), 25-40. https://doi.org/10.12989/gae.2022.29.1.025.

Soomro, M.A., Kumar, M., Mangi, N., Mangnejo, D.A. and Cui, Z. D. (2022b), "Parametric study of twin tunneling effects on piled foundations in stiff clay: 3D finite-element approach", *Int. J. Geomech.*, **22**(6), 04022079.

https://doi.org/10.1061/(ASCE)GM.1943-5622.0002386.

Soomro, M.A., Liu, K., Mangnejo, D.A. and Mangi, N. (2022c), "Effects of twin excavations with different construction sequence on a brick masonry wall: 3D finite element approach", *Structures*, **41**, 866-886. https://doi.org/10.1016/j.istruc.2022.05.060.

Tan, Y., Huang, R., Kang, Z. and Bin, W. (2016), "Covered semi-top-down excavation of subway station surrounded by closely spaced buildings in downtown Shanghai: Building response", *J. Perform. Constr. Fac*., **30**(6), 04016040. https://doi.org/10.1061/(ASCE)CF.1943-5509.0000892.

Wang, L., Cheng, W.C. and Xue, Z.F. (2022), "Investigating microscale structural characteristics and resultant macroscale mechanical properties of loess exposed to alkaline and saline environments", *Bull. Eng. Geol. Environ.*, **81**(4), 1-17. https://doi.org/10.1007/s10064-022-02640-z.

Xue, Z.F., Cheng, W.C., Wang, L. and Song, G. (2021), "Improvement of the shearing behaviour of loess using recycled straw fiber reinforcement", *KSCE J. Civil Eng.*, **25**(9), 3319-3335. https://doi.org/10.1007/s12205-021-2263-3.

Zhang, R., Zheng, J., Pu, H. and Zhang, L. (2011), "Analysis of excavation induced responses of loaded pile foundations considering unloading effect", *Tunn. Undergr. Sp. Tech*., **26**(2), 320-335. https://doi.org/10.1016/j.tust.2010.11.003.

Zhang, L.M. and Ng, A.M.Y. (2005), "Probabilistic limiting tolerable displacements for serviceability limit state design of foundations", *Géotechnique*, **55**(2), 151-161. https://doi.org/10.1680/geot.2005.55.2.151.

GC